Chinese Journal of
POLYMER SCIENCE

ARTICLE

https://doi.org/10.1007/s10118-021-2532-0
Chinese J. Polym. Sci. **2021**, *39*, 545–553

Reversible Mechanochemistry Enabled Autonomous Sustaining of Robustness of Polymers—An Example of Next Generation Self-healing Strategy

Ming-Xuan Li, Min-Zhi Rong*, and Ming-Qiu Zhang*

Key Laboratory for Polymeric Composite and Functional Materials of Ministry of Education, Guangdong Provincial Key Laboratory of High Performance Polymer Composites, School of Chemistry, Sun Yat-Sen University, Guangzhou 510275, China

Electronic Supplementary Information

Abstract Even under low external force, a few macromolecules of a polymer have to be much more highly stressed and fractured first due to the inherent heterogeneous microstructure. When the materials keep on working under loading, as is often the case, the minor damages would add up, endangering the safety of use. Here we show an innovative solution based on mechanochemically initiated reversible cascading variation of metal-ligand complexations. Upon loading, crosslinking density of the proof-of-concept metallopolymer networks autonomously increases, and recovers after unloading. Meanwhile, the stress-induced tiny fracture precursors are blocked to grow and then restored. The entire processes reversibly proceed free of manual intervention and catalyst. The proposed molecular-level internal equilibrium prevention mechanisms fundamentally enhance durability of polymers in service.

Keywords Metal-ligand complexations; Polyurethane; Mechanochemistry; Mechanical properties; Robustness

Citation: Li, M. X.; Rong, M. Z.; Zhang, M. Q. Reversible mechanochemistry enabled autonomous sustaining of robustness of polymers—an example of next generation self-healing strategy. *Chinese J. Polym. Sci.* **2021**, *39*, 545–553.

INTRODUCTION

It is well known that humans can cure cellular microdamage and non-fatal diseases or injuries through the internal equilibrium protection mechanisms. Self-healing of small wounds represents a typical example of these attractive functionalities, which has been duplicated in synthetic polymers for crack rehabilitation.[1–4] In fact, it may be equally or even more important for artificial materials to imitate the capability of organisms for removing hidden troubles before they develop into unstable damages or even catastrophic failures. To the best of our knowledge, however, the topic used to rarely get attention. There has not yet been report concerning such a next generation technique for polymers, focusing on autonomous elimination of the possibility of crack growth in the early stage whenever the tiny damage precursors originating from broken molecular chains are initiated, rather than re-bonding of broken parts after macroscopic failure.

The challenge of developing this type of smart material lies in the incorporation of appropriate stimulus-response mechanisms, which are mechanosensitive enough to lower stress and able to arrest cleavage of macromolecules under applied force at the same time and then re-bond the damaged portions.

Comparatively, the reversible metal-ligand interactions seem to be suited to fulfill the task.[5–9] Ultrasound-induced mechanochemical scission of a metal complex with polymeric ligands proved to produce either an active ligand that can catalyze transesterification or an active metal site that can catalyze polymerization.[6] Meantime, by mimicking the habits of mussel byssus,[10–14] synthetic polymer networks with the coordination bonds between 3,4-dihydroxyphenylalanine (DOPA) and ferric ions, or those between histidine (HIS) and zinc ions, as mechanically active cross-linkers acquired self-healability of macroscopic wounds,[15–18] and tunability of mechanical properties.[19–22]

Inspired by these explorations, here in this work we propose a proof-of-concept bulk metallopolymer capable of sustaining robustness of polymeric materials through mechanochemically initiated cascading variation of metal-ligand coordination interactions among macromolecules in the absence of manual intervention. As illustrated below (Fig. 1a) and in the electronic supplementary information (ESI) (Fig. S1), the target polymer is a polyurethane (PU, code name: HIS-DOPA-PU). Its soft segments and hard segments are crosslinked by HIS-Zn^{2+} and DOPA-Fe^{3+} complexations, respectively.

* Corresponding authors, E-mail: cesrmz@sysu.edu.cn (M.Z.R.)
E-mail: ceszmq@sysu.edu.cn (M.Q.Z.)

Received November 8, 2020; Accepted November 23, 2020; Published online December 9, 2020

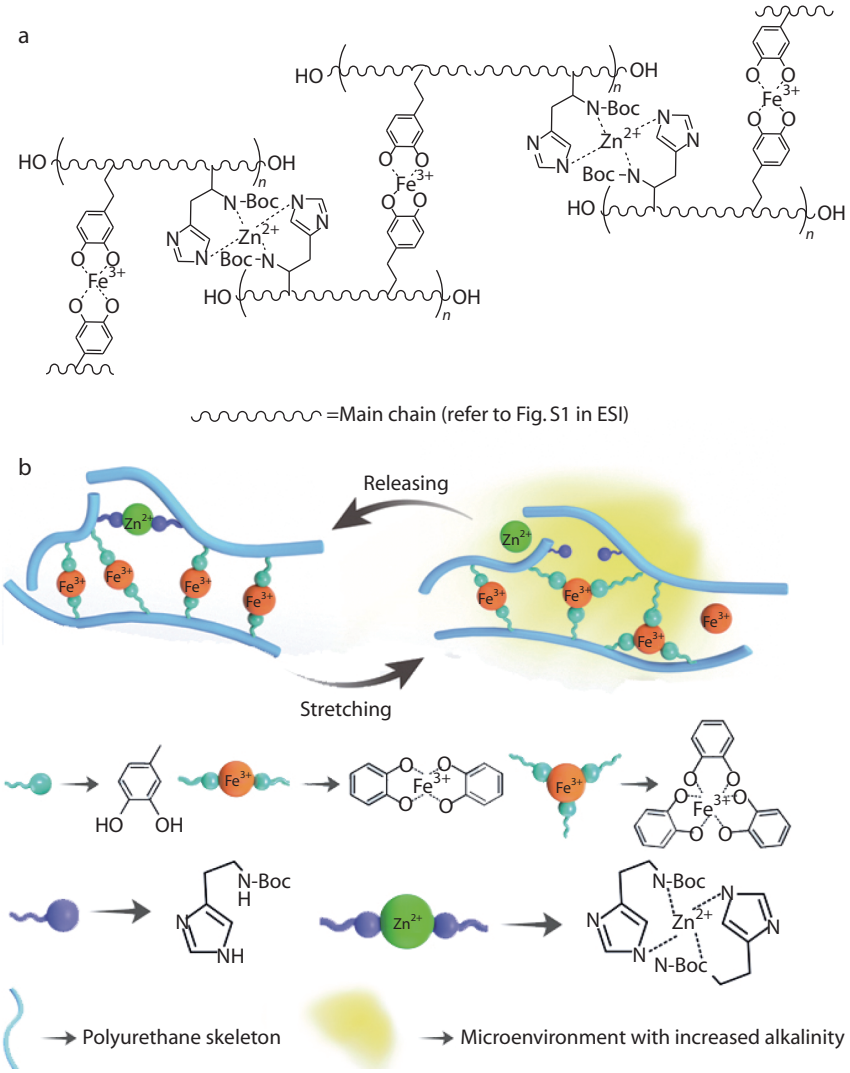

Fig. 1 Molecular design and working principle. (a) Structure of the proof-of-concept crosslinked polyurethane (HIS-DOPA-PU). (b) Schematic drawing of the mechanochemically initiated reversible cascading variation of the metal-ligand complexations.

Earlier study on DOPA-Fe^{3+} complexes indicated that their stoichiometry is pH dependent:[12,23,24] mono-species dominate at acidic pH, bis- from low acidic to low alkaline pH, and tris- at basic pH. HIS-Zn^{2+} is predominantly bis metal complex at pH 7 and mono-coordinated in a slightly acidified medium (pH=5.9).[16,25,26] Following the findings, the metal-ligand crosslinkages (*i.e.* HIS-Zn^{2+} and DOPA-Fe^{3+} bonds) of our polyurethane can be purposely tuned to be bis-complexations when the pH level of the polyurethane solution containing zinc and iron ions and the ligand/metal molar ratio are respectively set at 8 and 2/1 during synthesis. The resultant is called HIS(bis)-DOPA(bis)-PU hereinafter for the convenience of discussion. Meantime, the control, *i.e.* HIS(bis)-DOPA(tris)-PU with bis-coordinated HIS-Zn^{2+} and tris-coordinated DOPA-Fe^{3+} (Fig. S1 in ESI), is prepared from almost the same compositions except for the Fe^{3+}/DOPA molar ratio of 1/3 and system pH of 10.

When force is applied (Fig. 1b), the weaker and mechanically active HIS-Zn^{2+} bonds[14,17,25,27,28] would be partially dissociated in preference to DOPA-Fe^{3+}. The imidazole rings of unbound free histidine ligands would increase pH of microenvironment of the material in the role of Lewis base, especially when the material is hydrated, favoring the transformation of neighboring bis-DOPA-Fe^{3+} bonds to the tris-coordination[29] according to the above-mentioned pH dependence of stoichiometry. By taking advantage of the contribution of the newly increased tris-complexation (*i.e.* additional crosslinking junctions), the stress level required for formation and growth of microvoids from accumulations of broken chain ends is raised, and the void coalescence is hindered. Although bond strength of tris-DOPA-Fe^{3+} is lower than that of bis-DOPA-Fe^{3+},[30] the increased crosslinking density of the polyurethane networks with a rise in the coordination number would enhance the materials' strength,[23] leading to blocking of crack growth.

Upon unloading, entropically favorable retraction of the stretched macromolecular networks leads to closure of the minor damages. Because of the spatial reconfigurability of co-

https://doi.org/10.1007/s10118-021-2532-0

ordination bonds that facilitates ligands exchange,[21] the imidazole rings of the unbound free histidine ligands residing in the soft segments of the polyurethane, which have higher mobility than the hard segments,[31] would associate with the nearby accessible Zn^{2+} to re-form HIS-Zn^{2+} bonds. The tiny wounds originating from breakage of HIS-Zn^{2+} interaction are thus restored.[17,27,32–34] Moreover, the decrease of the amount of the free imidazole rings would also reduce alkalinity of the system, and the tris-DOPA-Fe^{3+} complexes have to be recovered to the original bis-complexations.

The feasibility of the above design is verified as follows, starting from the basic understanding of the structure of the model polymer.

EXPERIMENTAL

Materials

Analytical grade polytetrahydrofuran (PTMEG, M_n=2000), isophorone diisocyanate (IPDI), dimethyl formamide (DMF), dibutyltin dilaurate (DBTDL), *n*-(*tert*-butoxycarbonyl)-L-histidine (Boc-L-histidine), dicyclohexylcarbodiimide (DCC), 1-hydroxybenzotriazole (Hobt), 2-amino-1,3-propanediol (SERINOL), dopamine hydrochloride, homocysteinthiolactone hydrochloride, sodium bicarbonate, tetrahydrofuran, ferric chloride, zinc chloride and triethylamine (TEA) were purchased from Sigma-Aldrich and used as received without further purification.

Characterization

Fourier transform infrared (FTIR) spectra were recorded using a Bruker EQUINOX55 spectrophotometer between 400–4000 cm^{-1} with a resolution of 4 cm^{-1} by the KBr sample holder method. At the last stage of the network preparation, the polymer solution was gently painted on the KBr holder.

Attenuated total reflection (ATR) spectra were collected with a Bruker TENSOR 27 spectrophotometer between 500 and 3500 cm^{-1} with a resolution of 4 cm^{-1}.

Proton nuclear magnetic resonance (^{1}H-NMR) spectra were obtained by a Bruker AVANCE III spectrometer (500 MHz) with dimethyl sulfoxide (DMSO-d) as solvent.

Raman spectra were collected by a confocal Raman microscope (ReinshawinVia). The diode-pumped 785 nm near infrared laser excitation was used in combination with a 20× microscope objective. The spectra were acquired using an air-cooled CCD behind a grating (300 g·mm^{-1}) spectrograph with a spectral resolution of 4 cm^{-1}. To avoid burning, the laser power of 10 mW and exposure time of 20 s were used for all the measurements.

Isothermal titration calorimetry (ITC) experiments were carried out with a Microcal VP-ITC and water was chosen as solvent. All titrations were performed at 303 K and the fitting of the measured data was performed with the analysis program of the Microcal instrument.

Dynamic mechanical analysis (DMA) was performed using a Mettler Toledo Instruments DMA SDTA861. For temperature sweeping tests, the specimens were cut into dumbbell shape (35 mm × 2 mm × 1 mm) and the tests were conducted in tension mode at a heating rate of 3 °C·min^{-1} under the frequency of 1 Hz. For frequency sweeping, the tests were conducted on the same type of specimens at room temperature.

Differential scanning calorimetry (DSC) tests were conducted on a TA Instrument DSC-Q10. The samples were first cooled to −65 °C and then heated to 100 °C at a rate of 10 °C·min^{-1} in nitrogen atmosphere. Two cooling-heating cycles were run in advance to eliminate the thermal history.

Stress relaxation tests were carried out on dumbbell shaped specimens (35 mm × 2 mm × 1 mm) with the same instrument as DMA at 25 °C in tensile mode at constant strain of 50% or 100%.

Tensile tests were conducted at 25 °C with a SANSCMT6103 universal tester using dumbbell shaped specimens (35 mm × 2 mm × 1 mm) at a crosshead speed of 50 mm·min^{-1}, unless otherwise specified.

Energy dispersive spectroscopy (EDS) analysis was performed by using a spherical aberration corrected transmission electron microscope (SAC-TEM, JEOL JEM-ARM200P). The samples were thin-sectioned by EM FC6 cryosection system (Leica) in advance.

X-ray photoelectron spectroscopy (XPS) study was carried out using a ThermoFisher ESCALAB XI^+ XPS instrument equipped with a monochromatic K*α* X-ray source. The conditions for all the survey scans were as follows: energy range=1361–0 eV, pass energy=100 eV, step size=1 eV, sweep time=270 s and X-ray spot size=500 μm × 500 μm.

Small angle X-ray scattering (SAXS) measurements were conducted on the Xenocs 2.0 instrument with MetalJet-D2 X-rays source (beam size=500 μm, wavelength=0.134 nm, exposure time=600 s). According to the standard procedures of data reduction, calibration and background correction, each 2D SAXS pattern was azimuthally averaged into a 1D SAXS profile as a function of the scattering vector $Q = 4\pi\sin(\theta/2)/\lambda$, in which θ is the scattering angle and λ is the X-ray wavelength.

To determine the swelling property, square-shaped samples were immersed in water at 25 °C for more than 48 h to ensure swelling equilibrium. Then, the samples were taken out and carefully wiped to remove the residual water. The swelling degree was determined from the following equation: $S = m_\infty/m_o$, where m_∞ is the weight of the swollen sample at the equilibrium state, and m_o is the weight of the dry sample.

Fatigue tests were conducted on an ADT-AV02 fatigue testing machine (Shimadzu) using precut samples.[35] An initial crack (4 mm) was introduced to the rectangular specimen (50 mm × 20 mm × 1 mm) by a razor blade. Then, the sample was clamped by the grips with a grip-to-grip separation of 10 mm, and cyclically deformed under a constant frequency of 0.5 Hz. To record the crack extension, we captured a photo of the sample every 10 s so that the crack length can be estimated by post-processing of the pictures.

Synthesis of Boc-L-histidine-diol and DOPA-SH-NH_2

Following the typical amidation procedures, Boc-L-histidine (5.00 g, 0.02 mol) and Hobt (0.54 g, 0.004 mol) were dissolved in dimethylformamide (DMF) in a flask under stirring. Then, SERINOL (2.18 g, 0.024 mol) was added. The solution was cooled to 0 °C, and DCC (5.00 g, 0.04 mol) dissolved in DMF in advance was added dropwise with stirring. Sealing the flask with rubber stopper, the reaction mixture was stirred overnight at room temperature. Afterwards, the solution was filtered and the crude product was purified by column chromatography (silica gel; eluent: 10% methanol in dichloromethane). Finally, a pale-

https://doi.org/10.1007/s10118-021-2532-0

yellow solid was obtained with the yield of 60% after evaporating the eluent. ^{1}H-NMR (500 MHz, DMSO-d, δ, ppm): 7.47–7.80 (1H, —CH=N—); 6.66–6.90 (1H, —CH=C); 6.09–6.39 (2H, —NH—); 3.80–4.00 (1H, —CH—); 3.27–3.72 (4H, —CH_2—); 2.87–3.14 (2H, —CH_2—); 2.62–2.87 (1H, —CH—); 1.00–1.48 (9H, —CH_3).[14,18]

DOPA-SH-NH_2 was prepared by slightly modifying a common method[31] to involve thiol group. Typically, dopamine hydrochloride (5.00 g, 0.026 mol) and homocysteinthiolactone hydrochloride (4.25 g, 0.027 mol) were dissolved in sodium bicarbonate aqueous solution. The solution was fluxed at 95 °C for 2 h and then saturated salt water was added. The mixture was extracted three times with tetrahydrofuran (THF). Afterwards, the solvent was removed, and the final product (yellow solid) was obtained by column chromatography (silica gel; eluent: 5% methanol in THF) with a yield of 70%. ^{1}H-NMR (500 MHz, methanol-d, δ, ppm): 6.55–6.73 (2H, —CH=); 6.39–6.51 (1H, —CH=); 3.11–3.35 (3H, —CH_2—, —CH—); 2.31–2.62 (4H, —CH_2—); 1.54–1.93 (2H, —CH_2—).[32]

Synthesis of HIS-DOPA-PU

PTMEG (10.00 g, 0.005 mol) was dissolved in DMF in a three-neck flask, and then DMF solution of IPDI (2.22 g, 0.01 mol) was added dropwise under nitrogen protection with mechanical stirring. Next, two drops of catalyst DBTDL were added and the prepolymerization was carried out at 60 °C for 5 h. Afterwards, Boc-L-histidine-diol (0.82 g, 0.0025 mol) was incorporated and the reaction kept on proceeding for 3 h. Eventually, the mixture was cooled down to 30 °C and DOPA-SH-NH_2 (0.67 g, 0.0025 mol) was added. The PU prepolymer was obtained after stirring for additional 3 h. Its structure was verified by FTIR spectrum (Fig. S2a in ESI). The bands at 1727 and 1525 cm^{-1} are the typical polyurethane signals for the amide structure (—NH—C=O) formed by IPDI and PTMEG. The absorption at 1727 cm^{-1} is assigned to C=O and that at 1525 cm^{-1} to —NH—. Besides, the band at 2888 cm^{-1} comes from the stretching vibrations of —$(CH_2)_2$— on the main chain of the polyurethane. As for the band at 3338 cm^{-1}, it represents the stretching vibration of —NH— of histidine, while the band at 747 cm^{-1} is attributed to the stretching vibration of catechol ring of dopamine.

Moreover, the ^{1}H-NMR spectrum (Fig. S2b in ESI) shows the following characteristic signals (δ, ppm): 7.55–7.69 (a, 2H, —CH= of imidazole ring), 6.82–6.95 (b, 3H, CH=CH of catechol), 4.05 and 4.5 (c, 1H, —NH— resulting from the reaction between NCO group and reactive hydrogen), 3.32 and 3.61 (d, 4H, —CH_2—CH_2— of all reagents), and 1.35–1.48 (e, 6H, —CH_3 of IPDI and histidine). The results demonstrate that histidine and dopamine groups have been successfully introduced into the polyurethane.

In the second phase of the synthesis, $ZnCl_2$ and $FeCl_3$ were employed to coordinate with HIS and DOPA groups, respectively, producing the dually crosslinked polyurethane in accordance to the approaches reported elsewhere.[15,16] Because HIS groups can only chelate divalent metal ions, and DOPA can form complex with divalent and trivalent metal ions, $FeCl_3$ (0.203 g, 0.00125 mol) was first added to the above PU prepolymer solution at the Fe^{3+}/DOPA molar ratio of 1/2, to avoid the coordination between DOPA groups and $ZnCl_2$. Having been stirred for 30 min, $ZnCl_2$ (0.168 g, 0.00125 mol) was added, and TEA was used to adjust the pH value of the system at 8. After partially removing the solvent, the remaining fluid was poured into a square silicone mold. The final HIS(bis)-DOPA(bis)-PU film was available when the residual solvent was evaporated in the drying oven.

For making the reference sample (*i.e.* HIS(bis)-DOPA(tris)-PU), as shown in Fig. S1 (in ESI), the same method was applied except that less $FeCl_3$ (0.135 g, 8.3×10^{-4} mol) was added at the Fe^{3+}/DOPA molar ratio of 1/3 and the system pH was increased to 10.

The successful formation of HIS-Zn^{2+} and DOPA-Fe^{3+} coordination bonds is evidenced by the Raman spectra in Fig. S2(c) (in ESI), in which the band at 1580 cm^{-1} represents the complexation between imidazole rings of histidine and Zn^{2+},[33] while those at around 500–660 cm^{-1} are attributed to the bis-coordinated DOPA-Fe^{3+}.[23] Additionally, there is a stronger band at 528 cm^{-1} on the spectrum of HIS(bis)-DOPA(tris)-PU, meaning that tris-state DOPA-Fe^{3+} has been formed.[23]

RESULTS AND DISCUSSION

The successful synthesis of the polyurethane used for the present work has been verified (Fig. S2 in ESI). The resultant HIS(bis)-DOPA(bis)-PU exhibits only a single T_g of the soft segment at −53 °C (Fig. S3 in ESI), meaning that the common microphase separation of polyurethane is suppressed. The analysis agrees with the measurements of small angle X-ray scattering (SAXS, Fig. S4 in ESI), where no significant phase can be distinguished except the metal ions clusters. In fact, the ion clusters are relatively well dispersed in the polymer (Fig. S5 in ESI), representing roughly homogeneous distribution of the metal-ligands crosslinks. Besides, the crosslinked polyurethane has rather low crystallinity of 1.1% (Fig. S6 in ESI), and the molecular weight between crosslinks, M_c, is 4.5×10^3 g·mol^{-1} (Fig. S7 and Table S1 in ESI).

To accomplish the research task, we first study the ultrasonically induced mechanoresponses of the solution of HIS(bis)-DOPA(bis)-PU prior to cast molding. The infrared spectra (Fig. S8a in ESI) show that the band of C—N bond of imidazole ring at 1260 cm^{-1} shifts to 1240 cm^{-1} after ultrasonication. The original strong electro-attracting Zn^{2+} of HIS-Zn^{2+} bond shortens the C—N bond length of imidazole ring so that the absorption appears at higher wavenumber. The subsequent mechanical breakdown of partial HIS-Zn^{2+} bonds allows a few Zn^{2+} to be separated from the imidazole rings and the C—N bond length returns to the unbound status as characterized by the appearance of the band at lower wavenumber. Consequently, the fraction of HIS-Zn^{2+} bonds decreases with the increasing ultrasonication time, and the system alkalinity increases due to appearance of the dissociated imidazole as characterized by the growing consumption of HCl for neutralization (Fig. 2a). Moreover, the tris-DOPA-Fe^{3+} bonds appear after ultrasonication as characterized by the Raman band at 528 cm^{-1},[21] while the absorption assigned to HIS-Zn^{2+} bonds at 1580 cm^{-1}[33] becomes weaker in comparison with the original version (Fig. S8c in ESI).

When the agitated solution was settled down for a while, these variations are slowly reversed (Fig. 2b and Fig. S8c in ESI). The results not only agree with the fact that HIS-Zn^{2+} bond has smaller association constant (Fig. S9 and Table S2 in

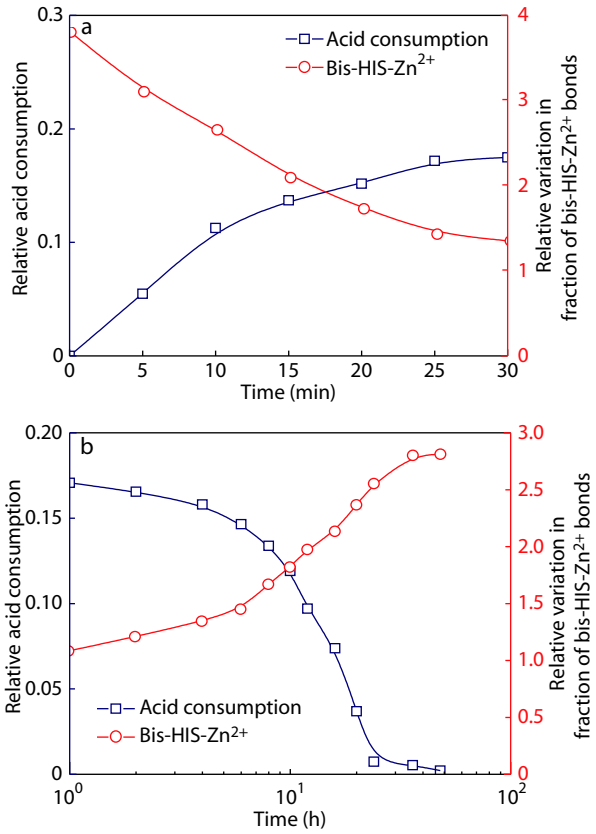

Fig. 2 Effect of ultrasonication on coordination status of HIS(bis)-DOPA(bis)-PU in DMF. (a) Ultrasonication time dependences of concentration variation of bis-His-Zn^{2+} bonds estimated from FTIR spectroscopy (Figs. S8a and S8b in ESI) and relative variation in the amount of HCl (0.1 $g{\cdot}L^{-1}$) consumed for neutralization. (b) The solution (that had been ultrasonically agitated for 30 min) was settled down for additional 30 min and then the same spectroscopic measurements and acid-base titration were conducted to check the concentration variations in bis-His-Zn^{2+} bonds and HCl consumption.

ESI), but also evidence that the mechanochemical dissociation of HIS-Zn^{2+} bonds releases imidazole, which increases environmental alkalinity and helps to build up tris-DOPA-Fe^{3+} coordination bonds. The cascading variations in the two metal-ligand coordination bonds and the resultant network rearrangement must be reversible accompanying application and removal of external force.

Interestingly, similar cascading effects are also found in the bulk material (Note: hereinafter a few specimens are immersed in water till saturation in advance (Fig. S10 in ESI) to trigger the dynamic reversibility of DOPA-Fe^{3+} interaction[12,36] and marked as hydrated). The redshift of the infrared band of C—N bond of imidazole from 1260 cm^{-1} to 1240 cm^{-1} appears again (Fig. 3a) when the specimen is stretched to 300% (which is much higher than the linear limit but far lower than the breaking point (Fig. S11 in ESI)). Further experiments manifest that the band position change is repeatable with cyclic loading (Fig. 3b) as the HIS-Zn^{2+} coordination is dynamically reversible,[17,27] and only detectable at larger strains (Fig. 3c1). The redshift could not be recovered so long as the deformation is fixed (*cf.* Figs. 3c2 and 3c3), meaning the force-induced alkalinity can last longer.

Such reversible variations in the coordination bonds in response to the same deformation are perceived by Raman (Figs. 3d–3f) and X-ray photoelectron spectroscopic studies (XPS, Figs. 3g–3l, Figs. S12 and S13 in ESI). Particularly, the percent area of N-Zn peak decreases and that of Cl-Zn increases for the stretched specimen (*cf.* Figs. 3g and 3i), and then the peaks are recovered after unloading (Fig. 3k) due to the dissociation/re-association of HIS-Zn^{2+} bonds. In contrast, the Fe2p peak splits into three components (4O-Fe, 6O-Fe and Cl-Fe) under applied force (*cf.* Figs. 3h and 3j) with the former two representing mixed bis- and tris-DOPA-Fe^{3+} complexations. The estimation of the oxygen and iron atoms involved in the coordination indicates 4.72 O atoms per Fe atom (Fig. 3j), which also reveals the co-existence of bis- and tris-complexes. Moreover, the area of Cl-Fe becomes larger after stretching because some Fe^{3+} become free and then match up with Cl^{-1}. Interestingly, the spectra can get back to the original profiles so long as the specimen is not subjected to stress (Fig. 3l). As for the control specimen of HIS(bis)-DOPA(tris)-PU (hydrated) (Fig. S13 in ESI), the peak areas of Zn-N and Cl-Zn exhibit the same changing trend with stretching but the Fe2p peak keeps unchanged. It implies that the dissociation of HIS-Zn^{2+} bonds does not arouse the transformation of bis-DOPA-Fe^{3+} to tris-DOPA-Fe^{3+} as the DOPA-Fe^{3+} coordination of the specimens has already been saturated.

It is thus known that the desired mechanochemical mechanisms indeed work (Fig. 1b), which is supported by the mechanochemically increased crosslinking density (Table S1 in ESI). Accordingly, macroscopic mechanical behaviors of the smart material are examined hereinafter.

Because the early minor damages in a material are often too small to be inspected and their influence on mechanical performance is also undetectable by conventional methods, a group of specific experiments are designed to multiply their destructive effect (Fig. 4a). That is, the specimens of interests are repeatedly pre-stretched to a certain strain and then their strengths are measured. Since such pre-stretching would promote gradual extension of the tiny damages, the tensile strength ratio of the pre-stretched specimen to that of the original one gives the measure of robustness.

As can be seen from Fig. 4(b), the robustness values of HIS(bis)-DOPA(bis)-PU (hydrated) only slightly decrease even though the specimens had been pre-stretched to higher strains. It is understandable since the cascading effects between the dynamic reversible HIS-Zn^{2+} and DOPA-Fe^{3+} bonds can be triggered in this case, and the envisaged changes in coordination numbers are allowed to proceed in the tests. The development of the early minor damages resulting from preferential dissociation of a few weak HIS-Zn^{2+} bonds is firstly blocked by the increase of tris-coordinated DOPA-Fe^{3+} bonds (*i.e.* crosslinking density of the polyurethane) during pre-stretching (refer to Fig. S11 in ESI), which indicates that the polyurethane containing tris-DOPA-Fe^{3+} crosslinks possesses higher strength than that with bis-coordination[21]), followed by rehabilitation *via* reformation of HIS-Zn^{2+} bonds in the course of unloading. Consequently, the robustness (or the strengths) of the pre-stretched specimens seems to be nearly independent of the pre-stretching times at fixed pre-strains. The marginal decrease of robustness with a rise in pre-stretching strain at given pre-stretching time

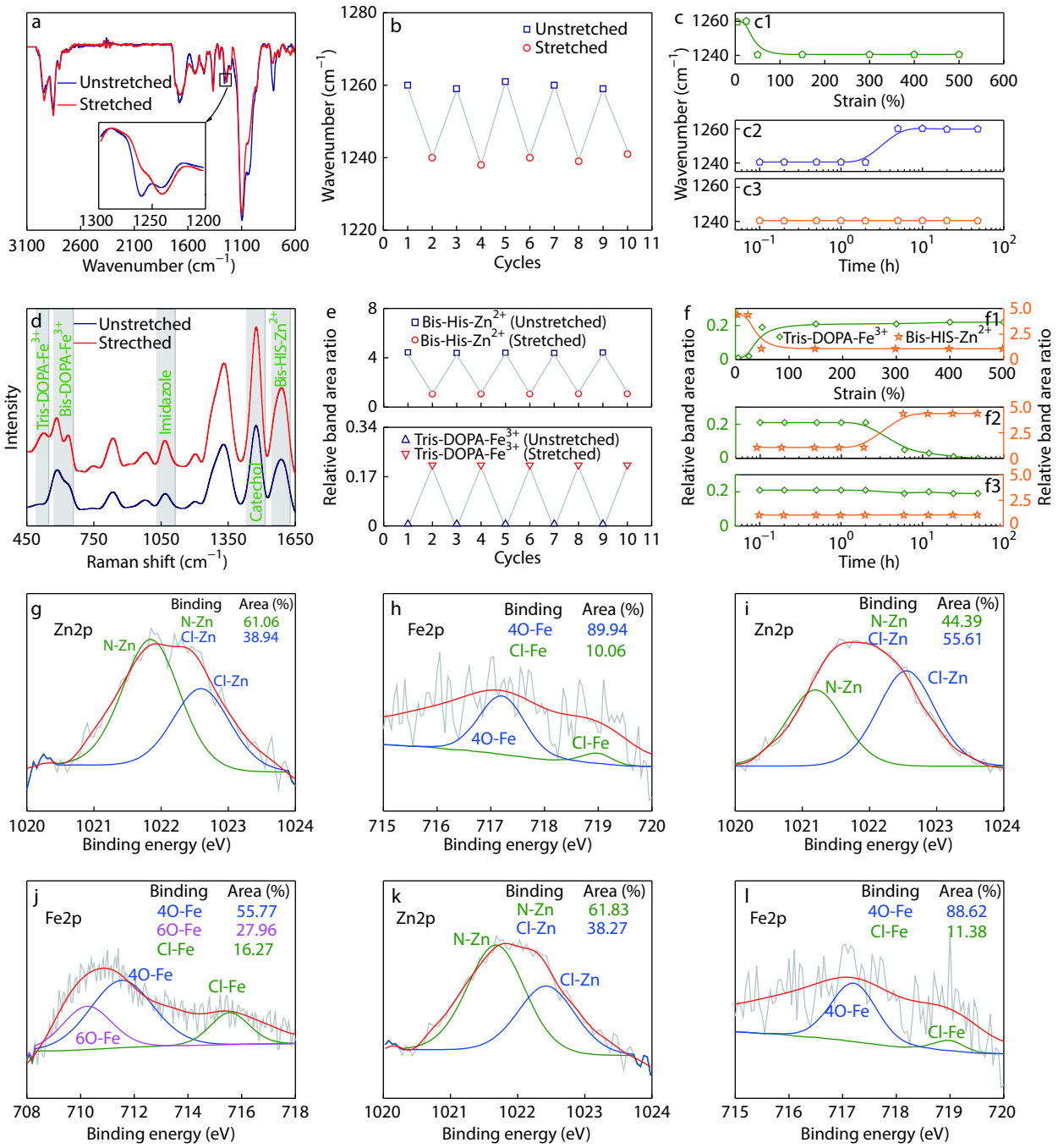

Fig. 3 Spectroscopic studies of HIS(bis)-DOPA(bis)-PU (hydrated). (a) Attenuated total reflection-Fourier transform infrared (ATR-FTIR) spectra. Effects of (b) repeated stretching, (c1) stretching strain, (c2) unloading after being stretched to the strain of 300%, and (c3) constant stretching strain of 300% on the infrared band position of C—N bond of the imidazole ring at 1240–1260 cm^{-1}. (d) Raman spectra. Effects of (e) repeated stretching, (f1) stretching strain, (f2) unloading after being stretched to the strain of 300%, and (f3) constant stretching of 300% on the area of the Raman band at 528 cm^{-1} of tris-DOPA-Fe^{3+} bonds and that at 1580 cm^{-1} of bis-HIS-Zn^{2+} bonds (in which the area of the band of catechol ring at 1480 cm^{-1}[24] and that of imidazole ring at 1080 cm^{-1}[17,26] serve as the internal standard references, respectively). (g) Zn2p XPS spectra of the original specimen. (h) Fe2p XPS spectra of the original specimen. (i) Zn2p XPS spectra of the stretched specimen. (j) Fe2p XPS spectra of the stretched specimen. (k) Zn2p XPS spectra of the unloaded specimen after stretching. (l) Fe2p XPS spectra of the unloaded specimen after stretching. Note: The measurements of the stretched specimens in (a), (b), (d), (e), (i) and (j) are conducted on the ones pulled to the strain of 300%.

should be attributed to the fact that the larger damages derived from more dissociated HIS-Zn^{2+} complexes under higher strain increase the difficulties of hindrance of crack growth and crack closure (Fig. S14 in ESI).

When the specimen is dehydrated, however, the amount of tris-coordination could not increase under the applied force as expected, even though mechanically induced dissociation of HIS-Zn^{2+} bonds still takes place. This is because the revers-

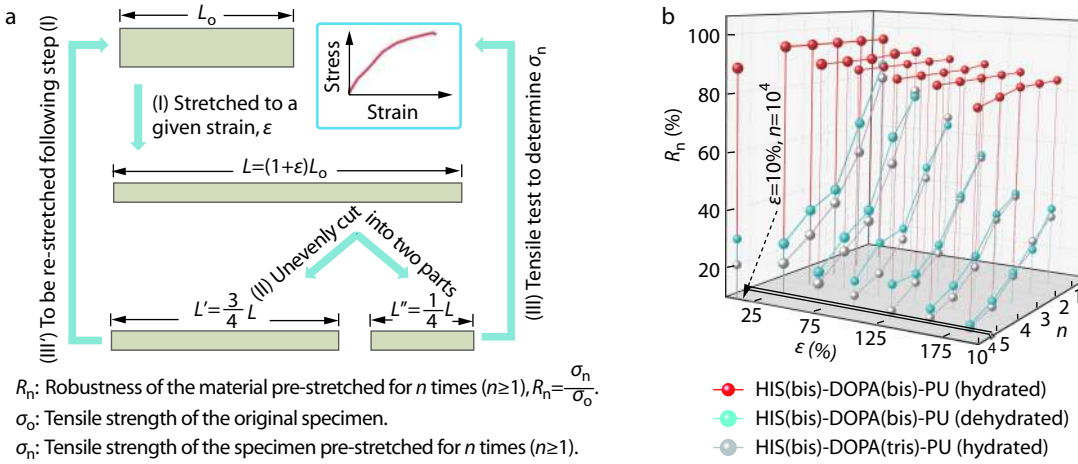

R_n: Robustness of the material pre-stretched for n times ($n\geq1$), $R_n=\frac{\sigma_n}{\sigma_o}$.
σ_o: Tensile strength of the original specimen.
σ_n: Tensile strength of the specimen pre-stretched for n times ($n\geq1$).

Fig. 4 Effect of pre-stretching on robustness. (a) Flow diagrams showing how the material is repeatedly pre-stretched and evaluated. Step (I): the specimen with original length of L_o is stretched to a constant strain of ε. Step (II): the pre-stretched specimen with the length L of $(1 + \varepsilon)L_o$ is unevenly cut into two parts. Step (III): tensile strength of the pre-stretched specimen, σ_n (in which n represents the pre-stretching times), is measured from the short segment (length $L'' = L/4 = (1 + \varepsilon)L_o/4$. Step (III'): the long segment (length $L' = 3L/4 = 3(1 + \varepsilon)L_o/4$) is stretched again following step (I) to start a new round of test. Note: crosshead speed for pre-stretching=50 mm·min^{-1}. (b) Robustness, R_n, of the polyurethanes pre-stretched to certain strain, ε, for different times, n. At the smallest strain of 10%, which is an exception, the specimens pre-stretched for up to 5 times did not show detectable decay of robustness. Therefore, they were repeatedly stretched for 10000 times *via* tension-tension fatigue under 0.5 Hz at the strain of 10% instead, prior to tensile tests.

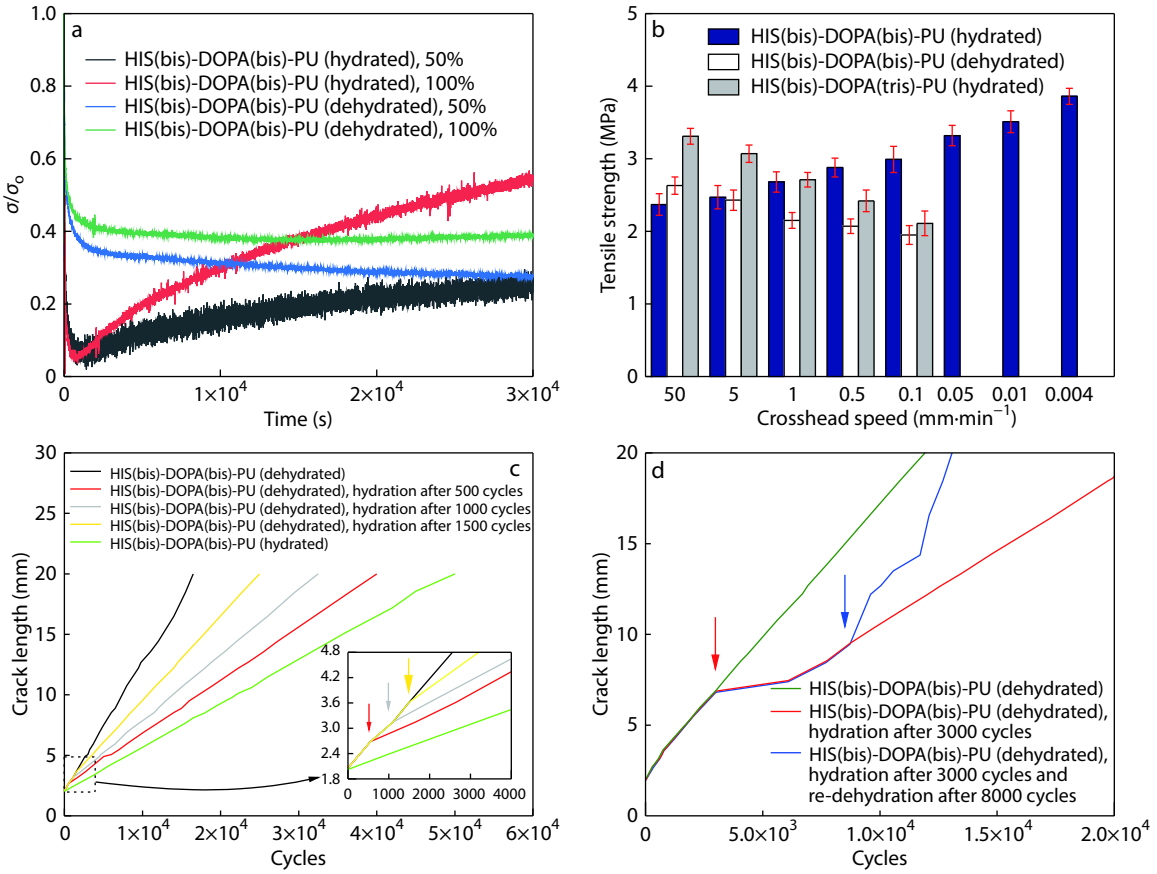

Fig. 5 Unusual mechanical behaviors. (a) Stress-relaxation behaviors measured at different strains. (b) Tensile strength versus crosshead speed. (c) Crack length versus fatigue cycles. For the dehydrated specimens, the tests were paused after certain cycles, and the specimens were wrapped by the absorbent cotton saturated with water for 12 h. (d) Crack length versus fatigue cycles. The *in situ* hydration of the specimen was conducted following the same procedures as described in (c). The re-dehydration was done by wrapping the specimen with the absorbent cotton saturated with absolute ethanol for 12 h. Volatilization of alcohol took away water from the specimen.

https://doi.org/10.1007/s10118-021-2532-0

ible DOPA-Fe^{3+} bonds are immobilized under the circumstances.[36] As a result, uncontrolled growth of the minor damages originating from dissociated HIS-Zn^{2+} interaction is enabled. Although the subsequent unloading-induced reconstruction of HIS-Zn^{2+} bonds might have more or less restored a few tiny damages, some larger ones remain unaffected probably due to the wider separation of the cracked surfaces. The robustness has to be significantly reduced with the pre-stretching strain and time. The results reveal the importance of mechanochemically aroused increase of tris-DOPA-Fe^{3+} bonds in obstruction of damage growth (*i.e.* self-blocking of minor damages) and the inability of HIS-Zn^{2+} bonds to recover larger wounds like other intrinsic self-healing strategies.[37] Similar phenomena are observed in another control (HIS(bis)-DOPA(tris)-PU (hydrated)). The DOPA-Fe^{3+} bonds should be reversible on the occasion, but the degree of coordination could not be changed since there is no bis-DOPA-Fe^{3+} complex. Besides, Fig. 4(b) suggests that supramolecular chemistry is not much helpful in maintaining the robustness as the materials have almost the same supramolecular interactions.

In fact, the mechanochemical enhancement of polyurethane networks is also reflected by the static stress relaxation tests (Fig. 5a). In contrast to the controls (dehydrated HIS(bis)-DOPA(bis)-PU), which behave like irreversibly crosslinked polymers, stress intensification rather than normal stress relaxation is observed with time for the specimens of hydrated HIS(bis)-DOPA(bis)-PU. The unusual behavior resembles other systems,[38–40] as the transient improvement of crosslinking density of the networks is triggered (Table S1 in ESI). Moreover, the larger pre-stretching strain corresponds to the steeper slope of the stress versus time. It means that more HIS-Zn^{2+} bonds are broken, rippling to a wider range of DOPA-Fe^{3+} so that more bis-DOPA-Fe^{3+} complexations transform into the tris-versions.

Besides Fig. 5(a), the time dependent mechanochemical response can be found in Fig. 5(b). Tensile strengths of the hydrated HIS(bis)-DOPA(bis)-PU specimens unprecedentedly decrease with increasing tensile speed, while the strengths of the controls change in the opposite direction as usual. Clearly, in case the external stress is applied within shorter time (*i.e.* higher tensile speed), many of the dynamic motifs in the former specimens are not ready for reaction, which leads to higher degree of stress concentration and lower strength, and vice versa. As for the controls, the mechanochemical transformation from bis-DOPA-Fe^{3+} to tri-coordination is not enabled so that their dependences of strength on tensile speed is not different from conventional polymers.

The plots of crack length versus fatigue cycles in Fig. 5(c) demonstrate that the dually crosslinked polyurethane can even retard development of existing crack under cyclic loading. The specimens of dehydrated HIS(bis)-DOPA(bis)-PU demonstrate that *in situ* absorption of water can remarkably decelerate the crack growth originating from partial dissociation of HIS-Zn^{2+} bonds and increase the fatigue life. Moreover, the earlier the water is added, the more prominent the improvement of fatigue resistance will be. It can be explained by the fact that the DOPA-Fe^{3+} bonds in the dehydrated specimens become activated after absorbing water, so that the network rearrangement that raises the stress level of microcracking is allowed at the crack tip. It is interesting to see that the reversible coordination is prohibited again with removal of water (Fig. 5d). The fatigue resistance of the specimen has to be lowered accordingly, since the transformation from bis-coordination to tris-coordination of DOPA-Fe^{3+} bonds can no longer proceed. The operating style of the material proves the occurrence of *in situ* mechanochemical self-strengthening.

CONCLUSIONS

Generally, the maximum service stress of a component should be only a fraction of the material's strength to ensure sufficient safety factor. Such an allowable stress design, which has been widely accepted in practice, seems to be not always valid for polymers as reflected by the present study. The pre-stretched strains (stresses) applied for determining robustness (Fig. 4) are obviously lower than the failure strain (strength) of the material (Fig. S11 in ESI), but the properties of the controls remarkably deteriorate with repeated pre-stretching due to accumulation and development of microcracks nucleated at the points of stress concentration in the inevitably uneven microstructures.[41] This is true even if the working stress is as low as ~3% of the strength (see the stress at ε=10% on the tensile curve of Fig. S11 in ESI). Only when both the two types of dynamic crosslinkages synergistically take effect, the property decline can be greatly hindered. It means that the capability of successive blocking and recovery of microcracks in the bud far before their spreading out, *i.e.* the capability of self-sustaining of robustness, should be an indispensable function of polymer materials. As for the self-healability of macroscopic damage (Fig. S15 in ESI), it is an inborn skill so long as the material is able to handle the fracture precursors as discussed above, which is not the focus of this work.

Electronic Supplementary Information

Electronic supplementary information (ESI) is available free of charge in the online version of this article at https://doi.org/10.1007/s10118-021-2532-0.

ACKNOWLEDGMENTS

This work was financially supported by the National Natural Science Foundation of China (Nos. 52033011, 51773229 and 51873235).

REFERENCES

1 White, S. R.; Sottos, N. R.; Geubelle, P. H.; Moore, J. S.; Kessler, M. R.; Sriram, S. R.; Brown, E. N.; Viswanathan, S. Autonomic healing of polymer composites. *Nature* **2001**, *409*, 794–797.
2 Chen, X. X.; Dam, M. A.; Ono, K.; Mal, A.; Shen, H.; Nutt, S. R.; Sheran, K.; Wudl, F. A thermally re-mendable cross-linked polymeric material. *Science* **2002**, *295*, 1698–1702.
3 Chen, X. X.; Zhong, Q. Y.; Wang, S. J.; Wu, Y. S.; Tan, J. D.; Lei, H. X.; Huang, S. Y.; Zhang, Y. F. Progress in dynamic covalent polymers. *Acta Polymerica Sinica* (in Chinese) **2019**, *50*, 469–484.
4 Yin, Q. Y.; Dai, C. H.; Chen, H.; Gou, K.; Guan, H. Z.; Wang, P. H.; Jiang, J. T.; Weng, G. S. Tough double metal-ion cross-linked elastomers with temperature-adaptable self-healing and

luminescence properties. *Chinese J. Polym. Sci.* **2021**, DOI: 10.1007/s10118-021-2517-z.
5 Paulusse, J. M. J.; Sijbesma, R. P. Reversible mechanochemistry of a Pd(II) coordination polymer. *Angew. Chem. Int. Ed.* **2004**, *43*, 4460–4462.
6 Kersey, F. R.; Loveless, D. M.; Craig, S. L. A hybrid polymer gel with controlled rates of cross-link rupture and self-repair. *J. R. Soc. Interface* **2007**, *4*, 373–380.
7 Piermattei, A.; Karthikeyan, S.; Sijbesma, R. P. Activating catalysts with mechanical force. *Nat. Chem.* **2009**, *1*, 133–137.
8 Balkenende, D. W. R.; Coulibaly, S.; Balog, S.; Simon, Y. C.; Fiore, G. L.; Weder, C. Mechanochemistry with metallosupramolecular polymers. *J. Am. Chem. Soc.* **2014**, *136*, 10493–10498.
9 Das, M.; Pal, S.; Naskar, K. Exploring various metal-ligand coordination bond formation in elastomers: mechanical performance and self-healing behavior. *Express Polym. Lett.* **2020**, *14*, 860–880.
10 Wilker, J. J. Marine bioinorganic materials: mussels pumping iron. *Curr. Opin. Chem. Biol.* **2010**, *14*, 276–283.
11 Harrington, M. J.; Masic, A.; Holten-Andersen, N.; Waite, J. H.; Fratzl, P. Iron-clad fibers: a metal-based biological strategy for hard flexible coatings. *Science* **2010**, *328*, 216–220.
12 Zeng, H.; Hwang, D. S.; Israelachvili, J. N.; Waite, J. H. Strong reversible Fe^{3+}-mediated bridging between DOPA-containing protein films in water. *Proc. Natl. Acad. Sci.* **2010**, *107*, 12850–12853.
13 Waite, J. H.; Qin, X. X.; Coyne, K. J. The peculiar collagens of mussel byssus. *J. Matrix Biol.* **1998**, *17*, 93–106.
14 Krauss, S.; Metzger, T. H.; Fratzl, P.; Harrington, M. J. Self-repair of a biological fiber guided by an ordered elastic framework. *Biomacromolecules* **2013**, *14*, 1520–1528.
15 Dzhardimalieva, G. I.; Yadav, B. C.; Singh S.; Uflyand, I. E. Self-healing and shape memory metallopolymers: state-of-the-art and future perspectives. *Dalton Trans.* **2020**, *49*, 3042–3087.
16 Zechel, S.; Hager, M. D.; Priemel, T.; Harrington, M. J. Healing through histidine: bioinspired pathways to self-healing polymers *via* imidazole–metal coordination. *Biomimetics* **2019**, *4*, 20.
17 Enke, M.; Bode, S.; Vitz, J.; Schacher, F. H.; Harrington, M. J.; Hager, M. D.; Schubert, U. S. Self-healing response in supramolecular polymers based on reversible zinc-histidine interactions. *Polymer* **2015**, *69*, 274–282.
18 Andersen, A.; Chen, Y.; Birkedal, H. Bioinspired metal-polyphenol materials: self-healing and beyond. *Biomimetics* **2019**, *4*, 30.
19 Tunn, I.; Harrington, M. J.; Blank, K. G. Bioinspired histidine-Zn^{2+} coordination for tuning the mechanical properties of self-healing coiled coil cross-linked hydrogels. *Biomimetics* **2019**, *4*, 25.
20 Filippidi, E.; Cristiani, T. R.; Eisenbach, C. D.; Waite, J. H.; Israelachvili, J. N.; Ahn, K.; Valentine, M. T. Toughening elastomers using mussel-inspired iron-catechol complexes. *Science* **2017**, *358*, 502–505.
21 Mozhdehi, D.; Neal, J. A.; Grindy, S. C.; Cordeau, Y.; Ayala, S.; Holten-Andersen, N.; Guan, Z. Tuning dynamic mechanical response in metallopolymer networks through simultaneous control of structural and temporal properties of the networks. *Macromolecules* **2016**, *49*, 6310–6321.
22 Grindy, S. C.; Learsch, R.; Mozhdehi, D.; Cheng, J.; Barrett, D. G.; Guan, Z.; Messersmith, P. B.; Holten-Andersen, N. Control of hierarchical polymer mechanics with bioinspired metal-coordination dynamics. *Nat. Mater.* **2015**, *14*, 1210–1216.
23 Holten-Andersen, N.; Harrington, M. J.; Irkedal, H. B.; Lee, B. P.; Messersmith, P. B.; Lee, K. Y. C.; Waite, J. H. pH-induced metal-ligand cross-links inspired by mussel yield self-healing polymer networks with near-covalent elastic moduli. *Proc. Natl. Acad. Sci.* **2011**, *108*, 2651–2655.
24 Wang, J.; Liu, C.; Lu, X.; Yin, M. Co-polypeptides of 3,4-dihydroxyphenylalanine and L-lysine to mimic marine adhesive protein. *Biomaterials* **2007**, *28*, 3456–3468.
25 Fullenkamp, D. E.; He, L.; Barrett, D. G.; Burghardt, W. R.; Messersmith, P. B. Mussel-inspired histidine-based transient network metal coordination hydrogels. *Macromolecules* **2013**, *46*, 1167–1174.
26 Andersson, M.; Hedin, J.; Johansson, P.; Nordström, J.; Nydén, M. Coordination of imidazoles by Cu(II) and Zn(II) as studied by NMR relaxometry, EPR, far-FTIR vibrational spectroscopy and Ab initio calculations: effect of methyl substitution. *J. Phys. Chem. A* **2010**, *114*, 13146–13153.
27 Schmidt, S.; Reinecke, A.; Wojcik, F.; Pussak, D.; Hartmann, L.; Harrington, M. J. Metal-mediated molecular self-healing in histidine-rich mussel peptides. *Biomacromolecules* **2014**, *15*, 1644–1652.
28 Li, Y.; Wen, J.; Qin, M.; Cao, Y.; Ma, H.; Wang, W. Single-molecule mechanics of catechol-iron coordination bonds. *ACS Biomater. Sci. Eng.* **2017**, *3*, 979–989.
29 Yang, B.; Lim, C.; Hwang, D. S.; Cha, H. J. Switch of surface adhesion to cohesion by dopa-Fe^{3+} complexation in response to microenvironment at the mussel plaque/substrate interface. *Chem. Mater.* **2016**, *28*, 7982–7989.
30 Xu, Z. P. Mechanics of metal-catecholate complexes: the role of coordination state and metal types. *Sci. Rep.* **2013**, *3*, 2914–2920.
31 Mozhdehi, D.; Ayala, S.; Cromwell, O. R.; Guan, Z. Self-healing multiphase polymers *via* dynamic metal-ligand interactions. *J. Am. Chem. Soc.* **2014**, *136*, 16128–16131.
32 Enke, M.; Jehle, F.; Bode, S.; Vitz, J.; Harrington, M. J.; Hager, M. D.; Schubert, U. S. Histidine-zinc interactions investigated by isothermal titration calorimetry (ITC) and their application in self-healing polymers. *Macromol. Chem. Phys.* **2017**, *218*, 1600458.
33 Enke, M.; Bose, R. K.; Zechel, S.; Vitz, J.; Deubler, R.; Garcia, S. J.; Zwaag, S. V.; Schacher, F. H.; Hager, M. D.; Schubert, U. S. A translation of the structure of mussel byssal threads into synthetic materials by the utilization of histidine-rich block copolymers. *Polym. Chem.* **2018**, *9*, 3543–3551.
34 Harrington, M. J.; Gupta, H. S.; Fratzl, P.; Waite, J. H. Collagen insulated from tensile damage by domains that unfold reversibly: *in situ* X-ray investigation of mechanical yield and damage repair in the mussel byssus. *J. Struct. Biol.* **2009**, *167*, 47–54.
35 Tang, J. D.; Li, J. Y.; Vlassak, J. J.; Suo, Z. G. Fatigue fracture of hydrogels. *Extreme Mech. Lett.* **2017**, *10*, 24–31.
36 Xia, N. N.; Xiong, X. M.; Wang, J.; Rong, M. Z.; Zhang, M. Q. A seawater triggered dynamic coordinate bond and its application for underwater self-healing and reclaiming of lipophilic polymer. *Chem. Sci.* **2016**, *7*, 2736–2742.
37 Zhu, D. Y.; Chen, X. J.; Hong, Z. P.; Zhang, L. Y.; Zhang, L.; Guo, J. W.; Rong, M. Z.; Zhang, M. Q. Repeatedly intrinsic self-healing of millimeter-scale wounds in polymer through rapid volume expansion aided host–guest interaction. *ACS Appl. Mater. Interfaces* **2020**, *12*, 22534–22542.
38 Xia, N. N.; Rong, M. Z.; Zhang, M. Q.; Kuo, S. W. Stress intensification—an abnormal phenomenon observed during stress relaxation of dynamic coordination polymer. *Express Polym. Lett.* **2016**, *10*, 742–749.
39 Lei, Y. F.; Shan, S. J.; Lin Y. L.; Zhang, A. Q. Network reconfiguration and unusual stress intensification of a dynamic reversible polyimine elastomer. *Polymer* **2020**, *186*, 122031.
40 Fortman, D. J.; Brutman, J. P.; Cramer, C. J.; Hillmyer, M. A.; Dichtel, W. R. Mechanically activated, catalyst-free polyhydroxyurethane vitrimers. *J. Am. Chem. Soc.* **2015**, *137*, 14019–14022.
41 Liu, C.; Lafdi, K.; Chinesta, F. Durability sensor using low concentration carbon nano additives. *Compos. Sci. Technol.* **2020**, *195*, 108200.